



PONTIFICIA UNIVERSIDAD CATÓLICA DE CHILE
ESCUELA DE INGENIERÍA

**OPTIMIZATION OF TEMPERATURE,
TARGETS, AND ILLUMINATION FOR HIGH
PRECISION PHOTOGRAMMETRIC
CAMERA CALIBRATION**

LOUISE CHANTAL DAUVIN GUTIÉRREZ

Thesis submitted to the Office of Research and Graduate Studies
in partial fulfillment of the requirements for the degree of
Master of Science in Engineering

Advisors:

LEONARDO VANZI

Santiago de Chile, June, 2017

© MMXVII, LOUISE DAUVIN GUTIÉRREZ



PONTIFICIA UNIVERSIDAD CATÓLICA DE CHILE
ESCUELA DE INGENIERÍA

**OPTIMIZATION OF TEMPERATURE,
TARGETS, AND ILLUMINATION FOR HIGH
PRECISION PHOTOGRAMMETRIC
CAMERA CALIBRATION**

LOUISE CHANTAL DAUVIN GUTIÉRREZ

Members of the Committee:

LEONARDO VANZI

MIGUEL TORRES

PABLO ZEGERS

JULIO VERGARA

Thesis submitted to the Office of Research and Graduate Studies
in partial fulfillment of the requirements for the degree of
Master of Science in Engineering

Santiago de Chile, June, 2017

*To my family and friends:
To those who have gone,
To those who have arrived,
To the unconditional ones,
And to the furry ones*

ACKNOWLEDGEMENTS

I would first like to thank my advisor, Professor Leonardo Vanzi for his guidance and help since undergraduate studies. During this period, he introduced me to the astronomical area, included me in this great project called MOONS, and also encouraged me to enter the Master program. I express him my gratitude for helping me in the preparation and correction of this thesis too.

Besides, I am grateful to AIUC members and particularly to the Instrumentation group for their daily tips and help. I also thank the guidance and academic advises of the Photogrammetry team of AIUC. This thesis has also been possible due to their comments and help in the definition of the plan to study camera calibration and photogrammetry. A special thank goes to Holger Drass, who has helped and supported me since my beginnings in MOONS. I really appreciate his advises, contacts and the work we have developed together. I also thank him, as well, for providing information, reading and making comments for this thesis.

Further, I am very grateful to all friends of mine whom I met in PUC and high school. I will never forget their help, the time they took to listen to me and the meetings which helped to ease the stressing and difficult moments. I should also point out my thankfulness for the works, circuits, projects and study we made together.

I must finally show my great gratitude to my parents, brothers and sisters. They have always encouraged me to do my best, and have given me strength to accomplish my goals. I thank them all for their daily support, their advises and much more during these 7 years. I make a special recognition to my mother who unconditionally and with great courage helps me daily, and to my father who was the editor of this and many others of my works.

TABLE OF CONTENTS

ACKNOWLEDGEMENTS	iv
LIST OF FIGURES	vii
LIST OF TABLES	viii
ABSTRACT	ix
RESUMEN	x
1. INTRODUCTION	1
1.1. MOONS	2
1.1.1. MOONS outline	3
1.1.2. Metrology system	6
1.2. Astronomical metrology	7
1.3. Photogrammetry	9
1.4. Camera Calibration	10
1.4.1. Perspective projection geometry	11
1.4.2. Camera parameters	12
1.4.3. Calibration apparatus	13
1.4.4. Camera models	14
1.5. Calibration procedure	17
1.5.1. Image acquisition	17
1.5.2. Target segmentation	18
1.5.3. Match 2D to 3D positions	19
1.5.4. Calibration computation	20
1.6. Measurement conditions	20
1.7. Hypotheses	21
1.8. Objectives	21

2. MEASUREMENT SETUP	22
3. TEMPERATURE OPTIMIZATION	24
3.1. Camera warm-up	24
3.2. Temperature stabilization	27
4. TARGETS CHARACTERISTICS OPTIMIZATION	30
4.1. Dependency on the target type	30
4.2. Convenient targets characteristics	31
5. ILLUMINATION OPTIMIZATION	34
5.1. Illumination and image quality	34
5.2. Illumination advices	35
6. CONCLUSIONS	37
REFERENCES	39

LIST OF FIGURES

1.1	MOONS instrument mounted on the telescope	4
1.2	Fibre Positioning Units	4
1.3	MOONS conceptual overview	5
1.4	Geometrical configuration of the MOONS metrology system	7
1.5	Perspective projection geometry for camera calibration	11
1.6	MOONS calibration targets in the World Coordinate System	14
1.7	Pinhole model for camera calibration	15
2.1	Experimental laboratory setup	23
3.1	Warm-up effect	24
3.2	Histograms of drifts without pixel clock compensation	25
3.3	Drifts of targets positions due to temperature variations per image	26
3.4	Drifts of targets positions after pixel clock compensation	27
3.5	Histograms of drifts after pixel clock compensation	28
4.1	Comparison of positions movements dependent on target characteristics when illumination angle changes 180°	32
5.1	Movement of target positions at different illumination intensities	35

LIST OF TABLES

1.1	MOONS instrument parameters.	3
-----	--------------------------------------	---

ABSTRACT

The Multi-Object Optical and Near-Infrared Spectrograph (MOONS) will be an instrument for one of the 8.2 m ESO Very Large Telescopes. MOONS will observe the spectra of 1000 objects in a 500 arcmin^2 field of view at the same time. To fulfil this challenge, a micrometric accuracy is required for the positioning of the optical fibres collecting the light from the astronomical objects. Hence, the movement of the Fibre Positioning Units and the calculation of the fibre positions in the focal plane of the telescope must be within a maximum error of $15 \mu\text{m}$. The measurement of those positions will be performed by a metrology system based on the photogrammetry technique.

Close-range photogrammetry uses digital cameras which are positioned nearby the measured object. The cameras must be calibrated in terms of their positions and optical properties. This is a crucial step in the complete metrology system, especially if micrometric precision is required. For that reason, the camera calibration must be performed in optimal room conditions.

In this research, the effect of temperature variations on the target positions was evaluated to be 0.1 pix during a warm-up period of 20 min or more. However, this effect was reduced to 0.02 pix and the warm-up period was decreased to less than 10 min by developing a controller for the camera's pixel clock. Additionally, a $\sim 22\%$ variation of illumination intensity implies a difference of 0.008 pix in the measurement dispersion. Other aspects studied here are the illumination angle and the target characteristics. A 180° movement of the illumination source with respect to the camera produces a 0.3 pix drift of the targets images when retroreflective targets are involved. In contrast, this effect is diminished ~ 10 times with the use of larger, opaque targets.

Keywords: Metrology, close-range photogrammetry, high-precision camera calibration, calibration conditions, temperature, illumination, calibration targets.

RESUMEN

MOONS, *Multi-Object Optical and Near-Infrared Spectrograph*, será un instrumento para uno de los telescopios de 8.2 m del *Very Large Telescope* de ESO. Este estudiará el espectro de 1000 objetos celestes en un campo de vista de 500 arcmin². Para ello ubicará micrométricamente un conjunto de fibras ópticas sobre la imagen de dichos objetos. El movimiento de las Unidades Posicionadoras de Fibra y el cálculo de sus posiciones deben tener un error menor a 15 µm. Este cálculo se realizará con un sistema de metrología basado en la técnica de fotogrametría.

La fotogrametría de rango cercano mide espacialmente objetos cercanos con cámaras digitales. Por ello, ellas deben calibrarse en términos de su posición y propiedades ópticas, lo que es crucial para el funcionamiento del sistema completo, más aún si se requiere precisión micrométrica. Por lo tanto, la calibración de cámaras debe desarrollarse en condiciones óptimas.

En esta investigación, el efecto de las variaciones de temperatura debido al calentamiento inicial de las cámaras, fue estimado como 0.1 pix de movimiento en las posiciones de los *targets* en las imágenes. Este efecto se redujo a 0.02 pix, al igual que el tiempo de calentamiento de las cámaras, que pasó de más de 20 minutos a menos de 10 minutos. Además, se estudió que una variación de 20% en la intensidad de la iluminación produce una diferencia de dispersión de medición de 0.008 pix. Asimismo se concluyó que 180° de variación angular de la iluminación y las cámaras produce variaciones de 0.3 pix con el uso de *targets* retroreflectantes. Por el contrario, estas variaciones se reducen ~10 veces con *targets* opacos de mayor tamaño.

Palabras Claves: Metrología, Fotogrametría de rango cercano, calibración de cámaras de alta precisión, condiciones de calibración, temperatura, iluminación, objetos para calibración.

1. INTRODUCTION

Studies of the sky are nowadays being carried out by means of large telescopes and high-tech instruments. This specialized technology for astronomy is developing fast and has allowed astronomers to discover new phenomena with a direct impact on the development of scientific theories. Astronomical instrumentation has been a powerful tool to study Earth's surroundings and far beyond. New advances in this area will help us to move both scientific and technological limits forward.

Astronomical studies are usually carried out with the information of the light received from the Universe. The large aperture telescopes fulfil the function of collecting as much light as possible and help to resolve astronomical objects that appear close to each other in the sky. The light from the sky is forwarded to different instruments such as cameras, spectrographs or interferometers. The data received from the instruments allows the analysis of the electromagnetic spectrum of the astronomical sources to gain knowledge on their chemical compositions, velocities, and temperatures.

With these motivations, the Astro-Engineering Center of the Pontificia Universidad Católica de Chile, AIUC, is leading the development and production of parts and entire, highly-competitive, astronomical instruments. In particular, this work is focused on the Multi-Object Optical and Near-Infrared Spectrograph (MOONS). In this interdisciplinary and intercontinental project, the AIUC team is focused on the metrology system of MOONS which is based on the photogrammetry technique.

The metrology system of MOONS has the purpose of measuring the position of the optical fibres that will be employed to receive the light of the astronomical sources to be studied. Inasmuch as the measurements of this metrology system are performed only depending on the information collected by a set of cameras, their properties must be very well known. The procedure to determinate these characteristics is called "Camera Calibration", which is crucial for the performance of the complete metrology system (Heikkilä & Silvés, 1997). Hence,

it is important to perform the calibration in optimal conditions (Muruganantham, Jawahar, Ramamoorthy, & Giridhar, 2009).

This research focuses on the characterization and optimization of the conditions for the camera calibration process of a close-range photogrammetry system. In particular, We studied the effects of temperature variations, illumination and characteristics of the calibration targets. The thesis is organized as follows: a detailed introduction to the metrology system and camera calibration is presented in Section 1; in Section 2, the experiments setup to analyse the optimal conditions is presented; Section 3 discusses the temperature effects on the measurements and a method to reduce them; Section 4 shows the targets characteristics effects and Section 5 the influence of the illumination intensity in the targets measurements; finally, the results are summarized in conclusions of Section 6. It is important to mention that Section 1 is dedicated to present an overview of the project and the following ones are part of a paper sent to a scientific journal.

1.1. MOONS

MOONS will be one of the third generation instruments for the ESO Very Large Telescopes (VLT's) at Cerro Paranal, II Region of Chile. This spectrograph will be mounted on one of the 8.2 m VLT's to analyse the sky in the wavelength range of $0.6\ \mu\text{m}$ to $1.8\ \mu\text{m}$ (Cirasuolo et al., 2014), which will be suitable to study both galactic and extragalactic astronomy. The instrument has two observational modes mainly. One high-resolution mode to study the stars in the Milky Way, and a second of medium-resolution which is dedicated to study faint galaxies. Due to these characteristics, MOONS would allow to perform an unprecedented census of the stars of our galaxy and to obtain, for the first time, a massive number of spectra for galaxies located beyond redshift 1. It will also contribute to the study of the evolution of the Universe and its beginnings, the study of the growth of galaxies and the chemical abundances of their stars, and it will also be helpful for monitoring the GAIA mission and the creation of a 3D model of the Milky Way (Cirasuolo et al., 2014).

A summary of MOONS most important characteristics is shown in Table 1.1, which will be discussed in the following subsections.

Table 1.1. MOONS instrument parameters.

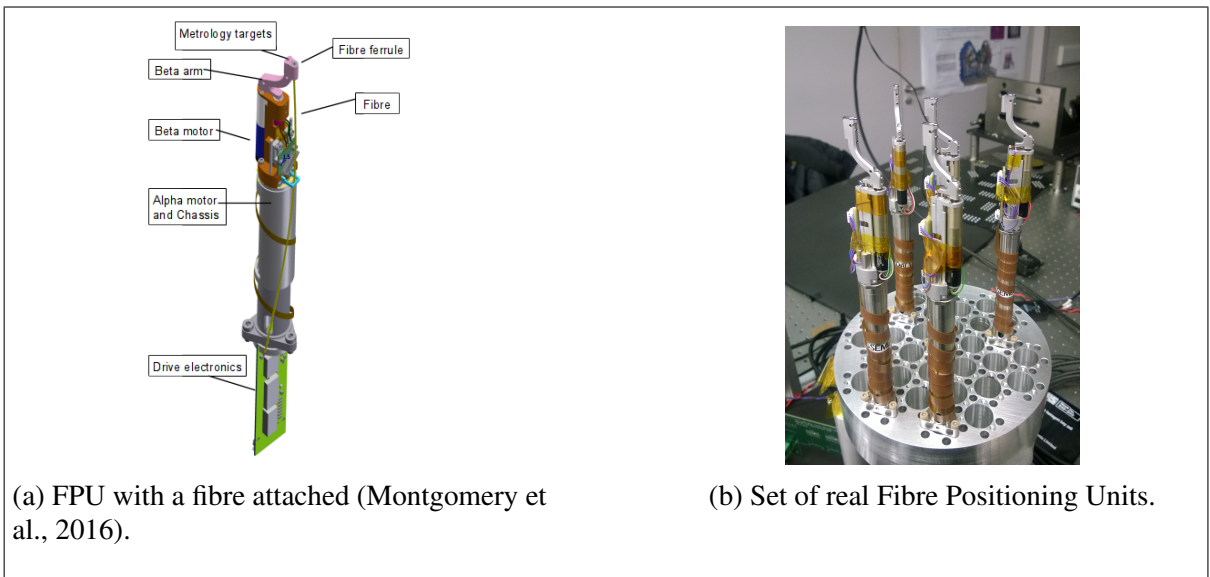
Telescope	8.2m, ESO VLT, Paranal, Chile	
Field of view	500 arcmin ²	
Throughput	30 %	
Number of optical fibres	1024	
Fibre diameter	150 μm	
Focal plane	Circular, 0.45 m radius	
Spectrographs		
	Medium-resolution mode	High-resolution mode
Resolution	4000 - 6000	RI band: 9000 YJ band: 4000 H band: 20000
Wavelength	0.64 μm - 1.8 μm	RI band: 0.76 μm - 0.9 μm YJ band: 0.95 μm - 1.35 μm H band: 1.52 μm - 1.63 μm
Metrology		
Metrology cameras	12 off-axis	
Illumination	24 LED arrays, off-axis	

1.1.1. MOONS outline

MOONS consists of a Rotating Front End (RFE) and a spectrograph mounted on Nasmyth platform of one of the VLTs. In general terms, the telescope first focuses the light from the sky in the Nasmyth focus, where 1000 astronomical objects are selected to be analysed. Then, this light travels through optical fibres from the RFE to a dual-arm spectrograph, which measure



Figure 1.1. MOONS instrument mounted on the telescope. The spectrograph is in the left, the front-end in the centre and one of the VLT's on the right (Cirasuolo et al., 2014).



(a) FPU with a fibre attached (Montgomery et al., 2016).

(b) Set of real Fibre Positioning Units.

Figure 1.2. The Fibre Positioning Units (FPUs) place the optical fibre on the images of the astronomical sources.

their spectra. In Figure 1.1 the telescope, the RFE and the spectrograph are presented and compared with the size of a person.

The 8.2 m telescope has the ability to observe the sky in a field of view (FOV) of 500 arcmin^2 and to focus its image in the focal plane. There, the light is received with a set of 1000 optical fibres in the RFE. The fibres are positioned in the focal plane on the astronomical sources with the help of 1000 robotic arms called Fibre Positioning Units (FPUs), presented in Figure 1.2. These FPUs consist of two Faulhaber DC-motors that perform the rotation of the so called alpha- and beta-arms. The beta-arms hold the fibres that forwards the light into the spectrograph. Finally, the light is dispersed in the two spectrograph arms, each arm is composed of three cameras designed to cover the different wavelength ranges. This schema is summarized in Figure 1.3, which shows the light path from the astronomical sources to the detectors where the spectra are recorded.

To accomplish a centring of the light on each fibre, the physical position of the beta-arms must be known and controlled very precisely. The image of the astronomical object must be very close to the centre of the $150 \mu\text{m}$ diameter fibre. The sky projected diameter of each fibre corresponds to 1.05 arcsec , hence, an accuracy of about 0.1 arcsec is required to ensure optimal observations. Therefore the accuracy of the beta-arms positioning must have

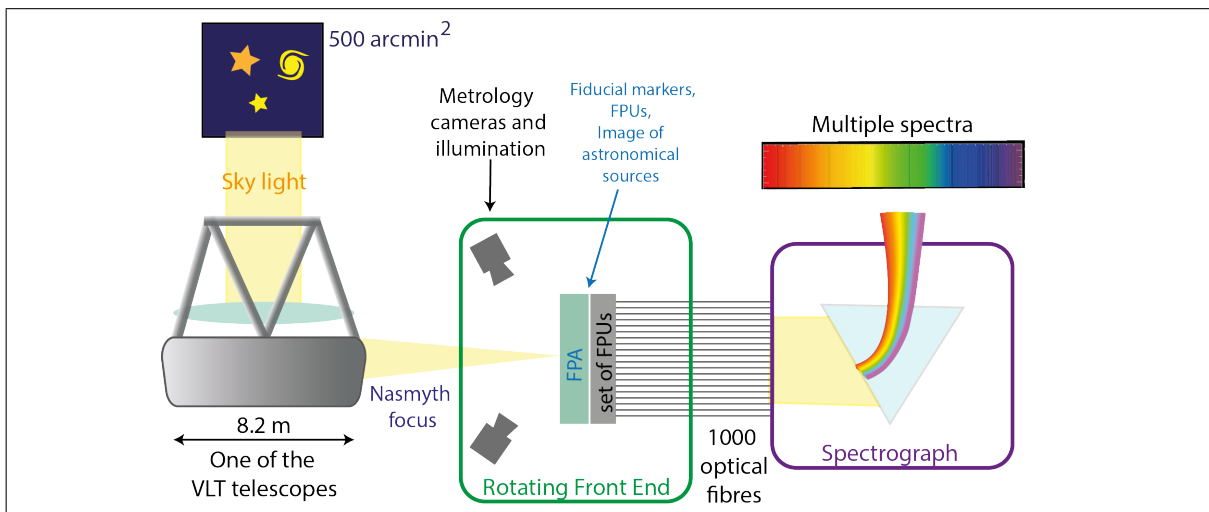


Figure 1.3. MOONS conceptual overview. The light from the sky is first received in the telescope, then, it passes to the Rotating Front-End in which 1000 astronomical objects are selected with optical fibre to be studied in the Spectrograph.

an uncertainty smaller than 15 μm . Both, measurement of the position of the FPUs and their movement must fulfil micrometric accuracy.

1.1.2. Metrology system

The purpose of the metrology system is measuring the beta-arms positions with high accuracy. It will be composed of a circular array of 12 off-axis metrology cameras, since on-axis cameras would obstruct the light path coming from the telescope. They will be placed at 560 mm from the focal plane due to the space limitations of the RFE. To cover the complete 0.45 m radius of the focal plane, the FOV of the cameras will overlap with each other (Drass et al., 2016). A IDS UI-3590 CP Rev-2 camera with a 4212 x 3648 pix sensor of 1.25 $\mu\text{m}/\text{pix}$ was selected in combination with an objective of 12 mm focal length to accomplish this requirement. Thus, the FOV of the cameras in the focal plane is 240 x 208 mm according to the pin-hole model:

$$\frac{1}{s_o} + \frac{1}{s_i} = \frac{1}{f} \quad (1.1)$$

$$\frac{h_i}{s_i} = \frac{h_o}{s_o} \quad (1.2)$$

Where f is the effective focal length, s_o and s_i the distance from the object and its image to the pin-hole, and h_o and h_i the sizes of the object and its image, respectively. Two lamps, one on each side of a camera, will illuminate the focal plane. Figure 1.4 shows the geometry of the metrology system for MOONS, where the cameras observe the focal plane in which the FPUs and reference targets are located.

The beta-arm positions will be measured by determining the position of a machined dots on the top of beta-arms, referred as metrology targets or targets from here on. The size of the image of a 3 mm target can also be estimated with 1.1 and 1.2. Thus, the image of that targets is 65 μm in the image plane of the camera, which corresponds to 52 pix in the a 1.25 $\mu\text{m}/\text{pix}$ sensor. Therefore, this sensor is suitable to sample well the metrology targets to allow a precise position determination.

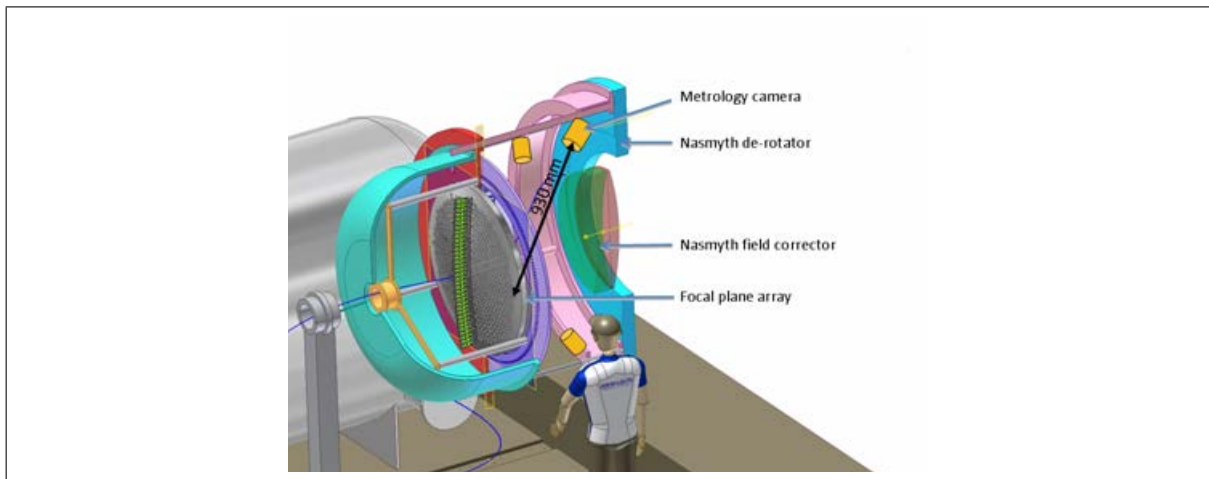


Figure 1.4. Geometrical configuration of the MOONS metrology system (Torres-Torriti et al., 2014). A set of 12 metrology cameras are disposed around the Focal Plane Array to determine the positions of the robotic arms.

Due to the optics of the telescope, the focal plane is curved (part of a sphere with 4 m diameter). The FPU's follow the curvature of the focal plane forming the Focal Plane Array (FPA). The targets will be recognized in the images taken with the cameras to then calculate the positions of the beta arms and with them the position of the fibres in the FPA. The FPA will also contain the fiducial markers, which are recognizable dot patterns that will reference the coordinate system.

It is important to mention that, since it is a high precision system and the instrument space is limited in the RFE, external mechanisms to heat or cool the cameras are difficult to include. Besides, the performance of external devices may exceed the temperature requirements of the RFE or introduce turbulences in the light path, which has to be avoided in the astronomical observations.

1.2. Astronomical metrology

Similar instruments have been developed to perform multi-object spectroscopy. Some of them are FLAMES, which entered to operation at one of the VLT's 15 years ago, and FMOS,

a recently decommissioned instrument at Subaru Telescope of Mauna Kea, Hawaii. As well as MOONS, other similar instruments will have their first light during the next years, e.g. PFS for Subaru Telescope, and 4MOST for ESO VISTA Telescope at Paranal.

All these instruments share with MOONS the characteristic of selecting the astronomical objects using optical fibres. PFS and 4MOST will select the astronomical sources with ~ 4000 optical fibres (Haynes et al., 2014; Tamura et al., 2016), and FLAMES with 560 fibres (Pasquini et al., 2002). However, MOONS is the only instrument with more than 1000 fibres and 2 DOF FPUs which is a great advantage to cover the telescope's focal plane.

In terms of metrology, they commonly use cameras in the telescope's light path. Frequently, back-illuminated fibres fed from a stable light source are seen in the focal plane, which light is projected to the metrology cameras through the telescope optics. In the case of PFS, a metrology camera of 50 Mpix and 380 mm aperture will be placed in the Cassegrain focus of the Subaru telescope. The camera size will allow for more resolution in the measurements of the optical fibres positions (S.-Y. Wang et al., 2016). On the other hand, 4MOST will guide the light to 4 folding mirrors that will reflect it to 4 metrology cameras (Winkler, Barden, & Saviauk, 2016).

On the contrary, MOONS is the first instrument that performs metrology with 12 cameras placed off-axis. This choice considers that cameras cannot obstruct the light path in the instrument configuration. This is beneficial to avoid interventions in both, the telescope and the light path. Besides, the measurements of the fibres positions are overdetermined by the intersection of 12 cameras FOVs. If one camera suffers damage, the metrology system can continue its performance.

Although these instruments are similar they have different objectives of study. Some of them study the southern and others the northern hemisphere; they also work at different frequencies in the ranges of optical and near-infrared wavelengths; and they have various FOV sizes in the sky.

1.3. Photogrammetry

The fast evolution of digital cameras and their sensors have made camera based metrology a widely used technique. In addition, digital sensors, the development of computing power, and efficient algorithms make image processing faster, more accurate, and reliable (Kang, Ha, & Jeong, 2008). Depending on the applications, camera based metrology is classified into two types: photogrammetry and computer vision. Even though photogrammetry and computer vision have similar applications, they present slight differences. Computer vision performs quick measurements in a completely automated manner, no matter how difficult to be recognized the measured scenes might be. Besides, this technique is less accurate in terms of precision and repeatability and uses low cost sensors (Muruganantham et al., 2009). In contrast, photogrammetry aims to get the highest precision of the measurements. It creates the need of having very well defined scenes and results verified by standard references (Luhmann, 2011). Applications such as face or patent identification, robot motion, object detection or motion recognition are examples of computer vision. On the other hand, several industrial, science, and engineering applications, such as MOONS, are photogrammetry instances. As MOONS requires micrometric precision measurements, the discussed metrology system is developed through the photogrammetry technique.

The term photogrammetry comes from the Greek words *phot*, that is translated as light; *gramma*, which means writing; and *metrein*, related to measurements. Hence, the term photogrammetry comprises the measurements of the “written” light. Although there is not an official definition, photogrammetry can be described as the science of obtaining reliable information from objects that are not in physical contact with the measuring instrument (Schenk, 2005).

Two big categories are found within photogrammetry, which are Aerial and Close-range photogrammetry. The difference between them lies in the range of closeness of the camera to the measured object. The first one uses images e.g. taken from planes or satellites far from the ground to investigate certain portions of the earth. On the contrary, Close-range

photogrammetry studies smaller objects with cameras located on earth e.g. in laboratories and industrial production. Here much smaller distances need to be resolved and this explains why Close-range needs to be more precise than Aerial photogrammetry.

There are variants of Close-range photogrammetry. The use of video instead of pictures to perform the measurements is one of them. Another is the use of either only one camera or a set of them to take pictures. The metrology system for MOONS is based on close-range photogrammetry with pictures and a set of 12 cameras.

1.4. Camera Calibration

The use of cameras for photogrammetry requires the knowledge of their physical and optical characteristics which determine the projection from real world to images. The process of obtaining this geometric relation is called “Camera Calibration”, and it is crucial in the performance of the complete photogrammetry system (Bacakoglu & Kamel, 1997; Kang et al., 2008; Luhmann, 2011; Zhang, 2000; Semeniuta, 2016). The accuracy and reliability of the camera calibration define, in most cases, the performance accuracy of the metrology applications (Heikkilä & Silvés, 1997; Swapna, Krouglicof, & Gosine, 2009), even more when they are high precision systems. Camera calibration can be a Self-calibration or a Photogrammetric calibration (Bazargani & Laganiere, 2015; Zhang, 2000). While Photogrammetric calibration needs an object to make the references to the real world, Self-calibration do not require any calibration apparatus. This last type is based on the fact that both the measured scene and the camera internal parameters are fixed, thus the calibration only needs few images. However, self-calibration is a new approach and its flexibility may compromise the precision of the method (Zhang, 2000; H. Wang, Shen, & Lu, 2012). On the other hand, Photogrammetric calibration is more suitable for high precision applications, but also more expensive due to the need of very precise calibration apparatus.

Camera characterization is carried out once, before using the metrology system. In the case of MOONS, Photogrammetric calibration will be performed in the instruments installation phase, as cameras should remain fixed all the time (Drass et al., 2016). Hence, camera position (extrinsic parameters), optical geometry (intrinsic parameters) and lens distortions are invariant at the moment of making measurements with MOONS.

1.4.1. Perspective projection geometry

The camera calibration is based on the projection geometry between the objects in the 3D and images space. Thus, three coordinate systems must be defined to understand it. These are the world coordinate system, the camera coordinate system and the image coordinate system (Bacakoglu & Kamel, 1997); which are presented in Figure 1.5.

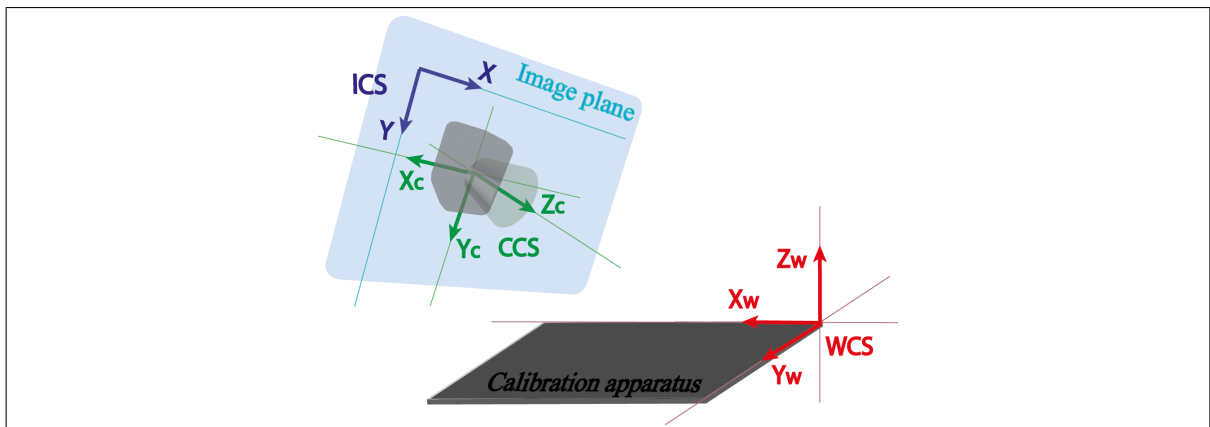


Figure 1.5. Perspective projection geometry for camera calibration. The metrology camera observes a planar apparatus which describes the World Coordinate System. It focuses the apparatus image in the image plane, which is defined the Image Coordinate System.

World coordinate system (WCS): This is the reference in the 3D real world, and it is defined in terms of the calibration object. There is no constraint to the orientation, except that the Z_w axis must be perpendicular to the planar apparatus (Samper, Santolaria, Brosed, Majarena, & Aguilar, 2013). It is defined with X_w , Y_w , and Z_w axes in Figure 1.5.

Camera coordinate system (CCS): It is a coordinate system whose centre is defined in the focus of the camera. Z_c axis of this reference is collinear to the optical axis (Bazargani & Laganier, 2015). It is defined with X_c , Y_c , and Z_c axes in Figure 1.5.

Image coordinate system (ICS): It is a 2D coordinate system that begins in the upper left corner of the image. It is measured in pixels of the sensor and defined with X and Y axes in Figure 1.5.

1.4.2. Camera parameters

The 2D-3D projective relation is described in terms of a set of extrinsic, intrinsic and distortion parameters. The so called “Extrinsic Parameters” are calculated to describe the camera location in the 3D world. They are defined as two vectors of position and orientation of the camera in terms of the WCS.

Likewise, the camera’s “Intrinsic Parameters” are the effective focal length, the centre point, and the scale factor. These correspond to the optical properties and internal geometry of the cameras, and due to their physical definition, are also called Physical camera parameters (Heikkilä & Silvés, 1997). The effective focal length (f_x, f_y) describes the optical focal of the camera measured in terms of the ICS. Besides, the centre point of the optics (c_x, c_y) is also measured in terms of X and Y axes and describes the intersection point of the optical axis with the image plane. Often, (c_x, c_y) does not correspond to the chip centre as the manufacturing process of the camera can be inaccurate. The last intrinsic parameter is the scale factor (s_x, s_y) , which depends on the pixel size in X and Y directions; in case it was a square pixel, then, $s_x = s_y$.

In addition, camera calibration also comprises the calculation of lens distortions. One of the first approaches of the distortion coefficients calculation was made by Brown, who included them theoretically and who also proved its importance empirically (Brown, 1971). Most authors describe lens distortion as two components, radial and tangential. Radial distortion is produced by Seidel aberrations and it is measured concentrically to the centre point.

In contrast, tangential distortion is produced by the misalignment of the curvature centres of the optics and measured tangentially to circles centred in (c_x, c_y) . Both radial and tangential distortions are modelled as polynomials, where each one of the coefficients represents the lens distortion parameters. Several researches do not include the distortion coefficients in the camera calibration model, others incorporate only radial distortion (Samper et al., 2013; Zhang, 2000) or only first coefficients inasmuch as some applications do not need the other ones (Bacakoglu & Kamel, 1997; Heikkilä & Silvés, 1997). However, when high precision is required, it is important to consider all distortions in the model.

1.4.3. Calibration apparatus

Commonly, the calibration makes use of a well known structure composed by a set of targets of easy identification. There exist two types of calibration objects: one which is a planar apparatus, where all targets are in the same plane; and another which is a three-dimensional structure with targets at different depth levels. Although the 3D apparatus provides high accuracy and reliability in the calibration, a precise manufacturing of it is often difficult to achieve. On the other hand, a 2D object, being of simple shape, brings less accuracy but it is more flexible and cheaper (Samper et al., 2013; Semeniuta, 2016). In addition, a 3D object is harder to handle and the different depths of the FOV, could lead to a defocus of some targets in the calibration images.

Several researches have proposed different types of targets, as for example circular patterns, chessboard corners, lines or surfaces (Luhmann, 2011). The most typical used pattern is chessboard whose lines intersections are used as targets (Samper et al., 2013). Circular targets are also widely used due to their simplicity and stability in their detection in the images as a result of the fact that the observed shape is the same from all points of view (Douxchamps & Chihara, 2009; Yang, Fang, Kong, & Li, 2014). Some other particular targets have been proposed in literature, as for example circle distributions (Kang et al., 2008), concentric rings (Yang et al., 2014), circles with lines passing through the centre (Adamos & Faig, 1992), among others.

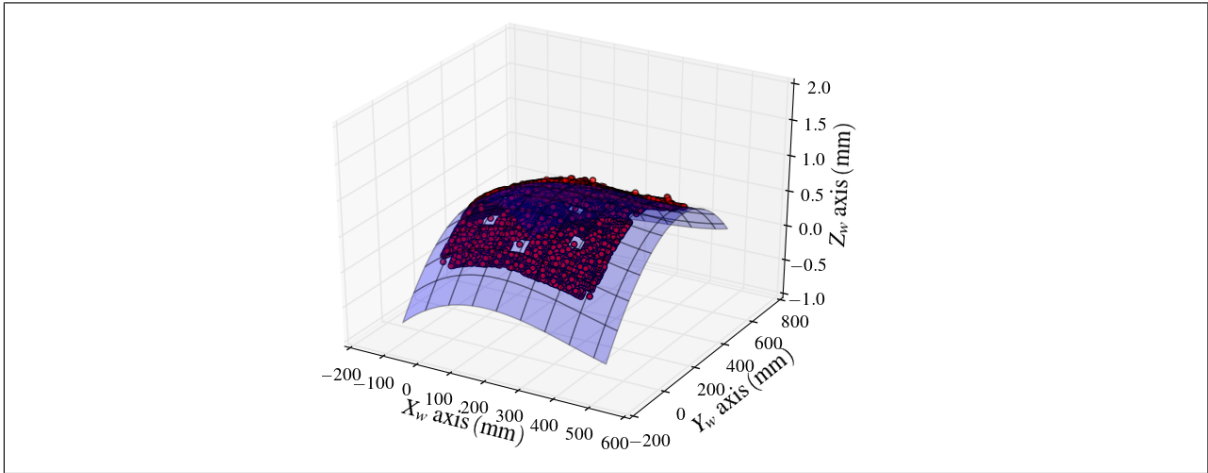


Figure 1.6. Calibration object targets in the World Coordinate System. A curvature is seen in the planar apparatus for MOONS cameras calibration.

Targets are also classified according to their response to illumination. They can be self-illuminated if illumination comes from the target itself, as for example an optical fibre fed with light. There are others which require external illumination, such as the retroreflective targets. These are composed by glass spheres which make light reflect in the same angle in which it arrived to the target (Feng, Li, Chen, & Li, 2009). The targets can also be non-retroreflectives, made of a opaque material that will reflect light in all directions (Shortis & Seager, 2014).

For the reasons previously discussed, a planar apparatus with circular targets was selected for the MOONS cameras calibrations. However, in the use of the calibration algorithm, the apparatus will be considered as a 3D object, instead of assuming that all targets are placed in a plane. This decision is based on the fact that the calibration object has some physical distortions that are not evident to human eye. Figure 1.6 shows the WCS positions of the calibration targets, which evidence a curvature of our planar calibration object.

1.4.4. Camera models

Many researchers have invested efforts in developing suitable calibration methodologies to improve the camera calibration process. In general terms, these calibration methods can be

classified into 3 categories, namely Linear, Non-linear, Two step methods; or other particular types.

Linear or direct methods are the more straightforward ones, they are based on the pinhole model, which describes in simple terms the ray trace of light as it passes through a pinhole, as seen in Figure 1.7. In other words, pinhole model assumes that light is projected in straight lines to the image plane (Heikkilä & Silvés, 1997).

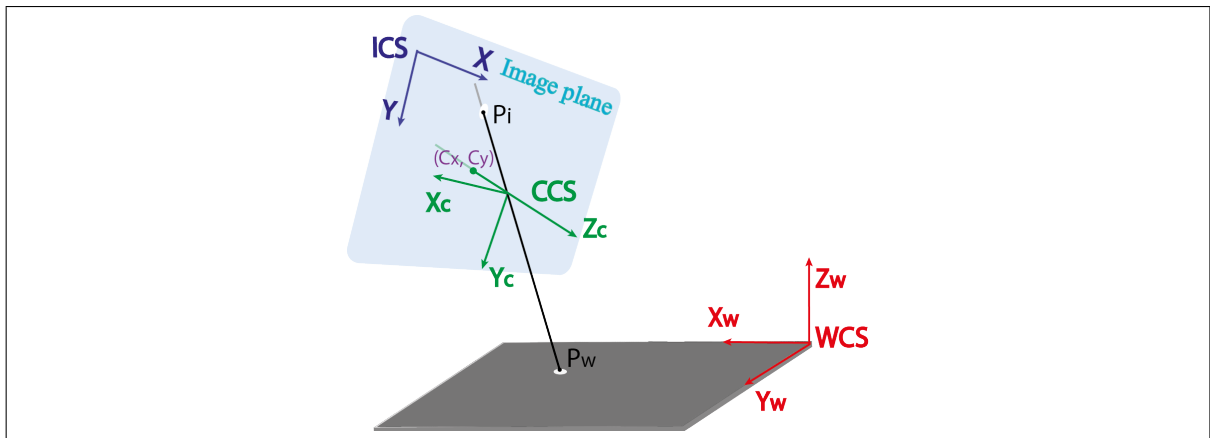


Figure 1.7. Pinhole model for camera calibration. The point P_w in the World Coordinate System is projected to P_i in the Image Coordinate System in a straight line that passes through the Camera Coordinate System origin.

Hence, a point of a 3D object in homogeneous coordinates of the WCS, $P_w = [P_{xw}, P_{yw}, P_{zw}, 1]$ will be projected to the image coordinate system as:

$$sP_i = CM \begin{bmatrix} R & | & t \end{bmatrix} P_w \quad (1.3)$$

Where, $P_i = [P_{xi}, P_{yi}, 1]$ is the projection of P_w to the ICS, and the rotation matrix R and the translation vector t describe the extrinsic parameters. This relation is also based on the Camera Matrix CM that includes the intrinsic parameters as seen in 1.4. The skew γ between axes X and Y can be neglected in most cases (Zhang, 2000).

$$CM = \begin{bmatrix} f_x & \gamma & c_x \\ 0 & f_y & c_y \\ 0 & 0 & 1 \end{bmatrix} \quad (1.4)$$

This systems can be resolved with different methods, such as the Direct Linear Transformation, DLT; or method of Hall. As linear methods are simple and do not require computational iterations, they are widely used in vision applications. Nevertheless, they are inadequate for high precision systems, due to the noise sensibility of the method and the neglected lens distortions (Bacakoglu & Kamel, 1997).

On the other hand, non-linear methods are more precise and reliable, since they are iterative and include lens distortions. They model radial (d_x^r, d_y^r) and tangential (d_x^t, d_y^t) distortions as seen in 1.5 and 1.6, where k_i and p_i are radial and tangential distortion coefficients, respectively, and $r_i = \sqrt{P_{xi}^2 + P_{yi}^2}$.

$$d_x^r = P_{xi} \sum_i k_i r_i^{2i} \quad d_y^r = P_{yi} \sum_i k_i r_i^{2i} \quad (1.5)$$

$$d_x^t = 2 p_1 P_{xi} P_{yi} + p_2 (r_i^2 + P_{xi}^2) \quad d_y^t = p_1 (r_i^2 + P_{yi}^2) + 2 p_2 P_{xi} P_{yi} \quad (1.6)$$

The distortions of the projection P_i are included in the model as the distorted image coordinates of point P_w , $(\widehat{P}_{xi}, \widehat{P}_{yi})$, as seen in 1.7 (Heikkilä & Silvés, 1997).

$$(\widehat{P}_{xi}, \widehat{P}_{yi}) = (P_{xi} + d_x^r + d_x^t, P_{yi} + d_y^r + d_y^t) \quad (1.7)$$

The non-linear methods aims to minimize the projection error, calculated as the difference between the image position of the targets and the calculated projection of the real positions of them in the WCS. Hence, the optimization problem is reduced to the expression shown in 1.8, where $P_{i jk}$ is the position of the target j of the image k in the ICS, and $\widehat{P}_{i jk}$ is the estimated projection from 3D to 2D of the same target.

$$\min \sum_j \sum_k \| P_{i_{jk}} - \widehat{P}_{i_{jk}} \| \quad (1.8)$$

This optimization can be resolved with methods such as the Levenberg-Marquardt optimization, the method of Faig, or the method of Paquette. Nonetheless, non-linear methods are computational expensive and requires a good initial guess to avoid local solutions. The problems of the methods are compensated with a combination of them. These are called two-step methods, which consist in computing a first approach of the parameters through a linear method, and then performing a non-linear optimization to minimize the projection error. Thus, the algorithm becomes more precise, reliable and less computationally expensive. Some of the most renowned of these methods are Tsai and Zhang (2000) methods (Samper et al., 2013). Other variations of the two-stage methods have also been proposed. For example a three-stage method, which includes an optimization of the rotational matrix (Bacakoglu & Kamel, 1997); or a four-stage method that corrects the ellipse centre and the distorted image coordinates (Heikkilä & Silvés, 1997).

1.5. Calibration procedure

The photogrammetric calibration process is a structured series of steps that begins with taking a set of images of the calibration object. The second step is the segmentation of each target in order to retrieve the object positions in each image. Once the image positions are known, it is necessary to recover a correspondence of the image objects with the real positions in the 3D world. These correspondences are necessary to perform the optimization of expression 1.8, which gives the camera parameters.

1.5.1. Image acquisition

The calibration images are obtained taking pictures at different angles of the calibration object. The larger the number of pictures acquired, the better the result achieved, since the non-linear optimization improves. The calibration algorithm requires avoiding degenerated

scenes, which are produced when the camera only is translated without rotations with respect to the object. The degenerated configuration does not contribute to the constraints in calibration method (Zhang, 2000).

1.5.2. Target segmentation

The second step of the camera calibration is the segmentation of targets in the images. First, all targets are detected and in a second step their positions are determined with sub-pixel precision.

This part of the calibration is of utter importance, since the following procedure is based on the targets positions (Douxchamps & Chihara, 2009; Semeniuta, 2016). Both accuracy and robustness of the system are also affected by this step (Semeniuta, 2016), thus it is crucial to perform segmentation in the most precise manner.

In order to detect and locate circular targets, some researchers have proposed to use direct approaches such as determining the centroids. This method consists of detecting the features and then performing a weighted mean with the intensity and position in the ICS (Feng et al., 2009). Centroid calculation is simple to follow but it is dependent on room conditions and target homogeneity (Ouellet & Hebert, 2007). Other researchers have proposed contour based segmentation, such as ellipse centre. This technique diminishes the perspective distortion produced when the camera takes pictures at high angles, which are measured from the normal of the targets (Ouellet & Hebert, 2007). Again a different group of authors have proposed to solve the skew problem of circle patterns with the inclusion of a correction of the ellipse centre in the camera model (Heikkilä & Silvés, 1997)

Centroid segmentation is performed during the calibration of the MOONS cameras using existing software suitable to perform the task. Two software packages DAOFIND as used in IRAF (Iraf, n.d.) and Source Extractor (SExtractor) (Bertin, 2014) were compared. It was concluded that SExtractor presented 0.02 pix less of deviation in the detection of simulated targets under noise and background conditions that were similar to the experimental images.

Besides, DAOFIND uses circles and SExtractor ellipses, thus SExtractor was selected to perform photometry on the calibration images (Drass et al., 2016). This open-source software is widely used in astronomy applications. As the circular white targets on a dark background are similar to astronomical images, SExtractor is suitable to determine the positions of the features in the images and store them in a text catalogue.

1.5.3. Match 2D to 3D positions

The calibration algorithm requires to know the match of the targets positions in the images and in the WCS. For that reason, the coordinates of the targets in the WCS must be known with micrometric precision to accomplish with the requirements of the photogrammetry system. A commercial photogrammetry system of Geodetic System Inc. (GSI) called “V-STARS N” (*V-STARS/N*, n.d.) is used to establish the WCS reference. This system is commonly used in surfaces measurements of antennas, and pieces inspection. V-STARS N consists of a high resolution camera, retroreflective targets stickers, scale bars and software for suitable data processing. To perform photogrammetry measurements with V-STARS N, the targets have to be stucked on the object that will be measured, and the scale bars at its side. Pictures of the object are then analysed in the PC, which computes the targets positions. This is very accurate system, that can reach down to $5\ \mu\text{m}$ precision in each direction of our calibration apparatus. Since the user has to take several pictures of the calibration pattern, the system is not fully automated, thus it is not suitable for the daily operation at the telescope. Besides, retroreflective targets must be placed on the measured object, which in MOONS case are beta-arms. However, it is a very helpful tool in the calibration process to calculate the 3D coordinates of the calibration targets.

The matching process of SExtractor and V-STARS N catalogues begins with the homography transformation of each image to fit the world coordinate system. The first task is recognizing certain points of the image (4 or more) that are correspondent to the same point in the real world. In order to achieve this, coded targets, delivered with V-STARS N, are used. They are known dot patterns easily recognizable in the images and in the 3D catalogue provided

by V-STARS N. With this information, the homography matrix is easily computed, and the positions of the targets in the image are mapped to an initial 3D position in the WCS. This is enough to find the nearest targets between the images and the V-STARS N catalogue. Finally, results are stored in a text file.

1.5.4. Calibration computation

The Zhang's two-step method has been modelled in MATLAB, by Jean-Yves Bouguet (2015), and extended to OpenCV (2016). This algorithms require the match between the ICS and the WCS to perform the calibration optimization. Thus, the camera calibration for MOONS will be performed through OpenCV, starting from the matches.

1.6. Measurement conditions

Even though camera calibration methods have been an active research field, little attention has been concentrated in the camera calibration conditions (Heikkilä & Silvés, 1997). Until now, researchers have studied the calibration targets (Douxchamps & Chihara, 2009), the geometry of the cameras (Handel, 2007), and the properties of the camera sensor, such as the dark current or the fixed pattern noise (Ortiz & Oliver, 2004; Healey & Kondepudy, 1994). However, the room conditions present at the time the images are acquired are also important since they affect the quality and segmentation of the images. This process may be compromised due to insufficient illumination, temperature differences, inaccurate calibration apparatus or mechanical perturbations. Consequently, it is important to make efforts in optimizing the conditions during camera calibration for a high precision photogrammetry system (Muruganantham et al., 2009).

Most of researchers prefer to include the measurement conditions corrections in camera model (Kang et al., 2008). Nevertheless, camera model and calibration methods become complicated and computationally intensive with the inclusion of more constraints and compensations. hence, we discovered that some environmental conditions such as temperature,

illumination and calibration apparatus characteristics can be precisely controlled to get a better segmentation of the images before the data analysis. The conclusions can also be extended to the entire measurement process of the metrology system.

1.7. Hypotheses

The hypotheses of this research is that certain characteristics such as illumination, temperature changes, target size, and the target's retro-reflectivity, introduce undesired uncertainties in the order of 0.5 pixel in the segmentation and position determination of the targets in the images. It is also proposed that this characteristics can be optimized in order to achieve a precision of less than 0.1 pix in the image segmentation.

1.8. Objectives

As a principal objective, this work aims at finding the optimal conditions required for the calibration of the MOONS cameras. Hence, the specific objectives of the research are: 1) Characterizing quantitatively the effects of illumination, temperature and target characteristics. 2) Finding methods to compensate these conditions. 3) Achieving a calibration of MOONS cameras that allows a precision within the requirements of the system.

2. MEASUREMENT SETUP

To evaluate the effects of the room conditions in the targets images positions, we propose a set of experiments to measure the relative drift of the targets in the ICS, and their measurement error, as a function of the environmental conditions and the target properties. In every test we keep the position of the camera and targets still, and vary a single environmental parameter, such as the camera temperature, the illumination orientation or intensity, or the physical properties of the targets. The tests setup includes:

Camera: A metrology CMOS camera, IDS UI-3590 CP Rev-2 in gray scale mode. Pixel size is $1.25 \mu\text{m}$, which ensures high resolution images.

Objective: A 8.5 mm KOWA camera objective.

Illumination: One Metz Mecalight LED light array (72 LEDs) controlled by an industrial PC called Beckhoff system; and One Metz Mecalight LED light array with a potentiometer to control light brightness, powered by an off-the-shelf network supply.

Targets: 3 mm and 6 mm non-retroreflective, and 3 mm retroreflective self-adhesive targets. They are circular white targets pasted on a dark carbon fibre plate.

Support plate: A carbon fibre plate with the pasted targets on an optical table, to ensure minimal vibrations and minimal thermal expansion.

Temperature controller: OMEGA[®] CSi8D.

Power-meter: Thorlabs PM320E.

The tests begin by continuously taking images of the targets for over one hour. The camera and the carbon fibre plate stay in the same position throughout the tests in order to guarantee constant measurement conditions, as seen in Figure 2.1. The tests are performed in a dark room, with the only illumination of the LEDs arrays. The position, brightness and shape of all circular white targets in the images are measured using Source Extractor (Bertin, 2014). This software is commonly used to analyse astronomical images, which are similar to the ones acquired in the calibration process and in the stability tests. Thus, the photometry of Source Extractor (SExtractor) proved to be suitable for that purposes.

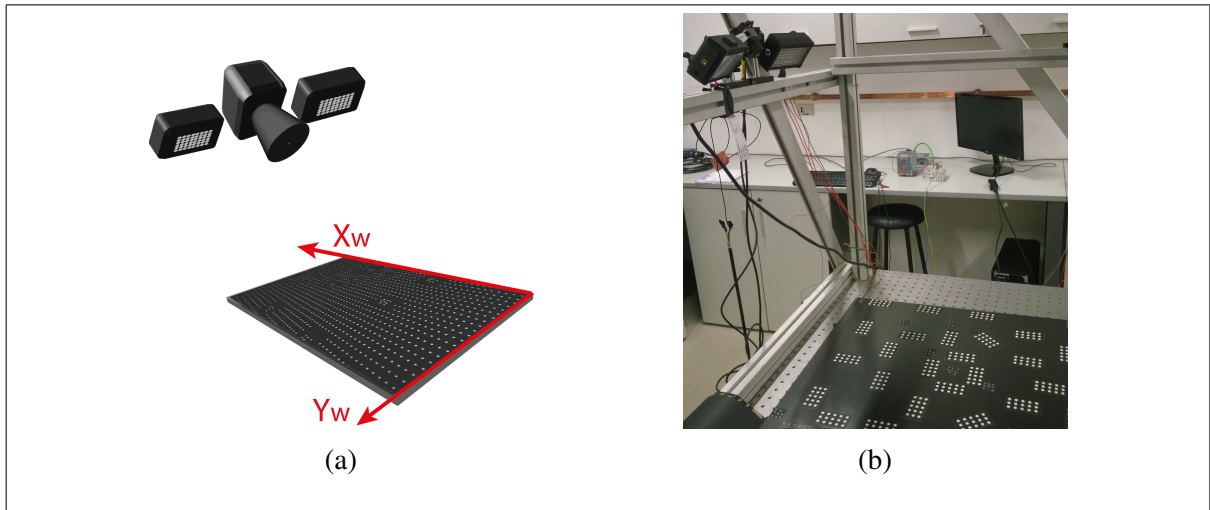


Figure 2.1. Experimental laboratory setup. The camera and calibration plate remain in their positions in the WCS.

The results are stored as a catalogue for each image which includes the Cartesian positions in the ICS in pixels. Then, every target position is compared to a reference catalogue. This one contains the ICS positions of the targets at the moment of the test set as reference. The difference of each catalogue to the reference is studied in terms of its standard deviation and average. The average is used to quantify systematic effects affecting the entire image, while the standard deviation is used to quantify measurement errors. The studied room conditions are varied one by one during the stability tests. Each tests details are explained in the correspondent sections.

According to our setup, the transformation of the drifts in the ICS to the camera image plane are defined by the pixel size of $1.25 \mu\text{m}/\text{pix}$. The translation of the ICS distances to the $Z_W = 0$ plane of the WCS are determined by the range of 86.25 to $126.98 \mu\text{m}/\text{pix}$, in accordance with the distance to the camera. However, these scales depend on the focal length, the pixel size and the position of the camera, thus all results will be presented in pixels.

3. TEMPERATURE OPTIMIZATION

3.1. Camera warm-up

The camera temperature increases during the acquisition of the first images after the camera has been turned on. This effect, called “camera warm-up”, takes several minutes before a constant temperature is achieved and produces a position drift in the targets positions on the order of 0.1 pix (Yu et al., 2014; Podbreznik & Potočnik, 2008; Handel, 2007; Sentenac, Maoultt, Rolland, & Devy, 2003; Smith & Cope, 2012). This is due to mechanical deformations of the optical geometry and changes of the refractive index of the lenses (Handel, 2007; Yu et al., 2014). An example of the change of temperature during camera warm-up is shown in Figure 3.1, where the temperature increases around 5 °C and then it stabilizes after the first 77 images. In this case, the temperature is considered stable having less than 3 % of variation. Since the images are taken at 4.35 frames / minute, it takes 18 minutes to stabilize the camera temperature.

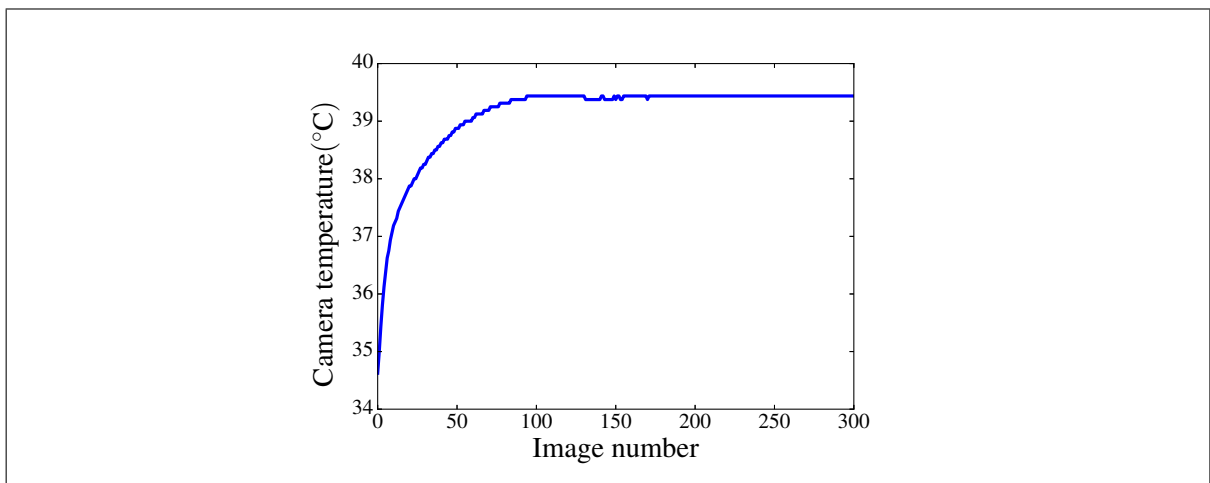


Figure 3.1. Warm-up effect. Temperature evolution depending on the number of images taken.

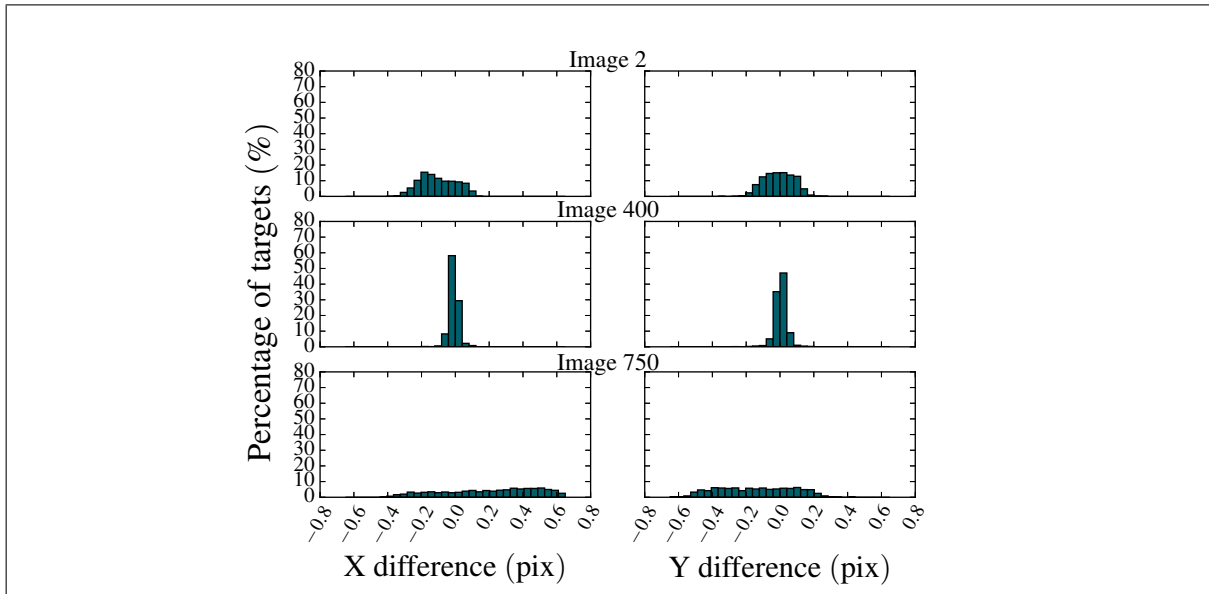


Figure 3.2. Histogram of the differences to the reference in 3 representative images at different temperatures. First row (image 2) represents the camera warm-up period, second row (image 400) the constant reached temperature, and third one (image 750) the external heated temperature. Image number 360, corresponding to stable temperature, was set as reference.

This problem was evidenced in the movement of the targets positions in the stability test. During it, we first waited until the temperature of the camera stabilized, and then warmed it up more using an external heater. The camera sensor temperature was stored in the header of the FITS format images. The results are shown in Figure 3.2, where the first row shows an histogram of the drifts during the warm-up; the second row, during the constant temperature, and the third one, after the external heating.

As seen in Figure 3.3, the 4.76 ± 0.06 °C exponential temperature variation during the camera warm-up period produces a drift of 0.09 ± 0.01 pix in Y axis and of 0.11 ± 0.01 pix in X axis. A similar behaviour is seen when temperature is increased on purpose, more targets have a high drift when temperature changes. When the heater is used, the sensor temperature goes up by 6.06 ± 0.06 °C, and the drifts in X and Y axes are 0.18 ± 0.01 pix and 0.17 ± 0.01 pix, respectively. Both results lead a drift rate of the measured targets positions in the range of 0.02 pix/°C to 0.03 pix/°C. In the same plots, the standard deviation

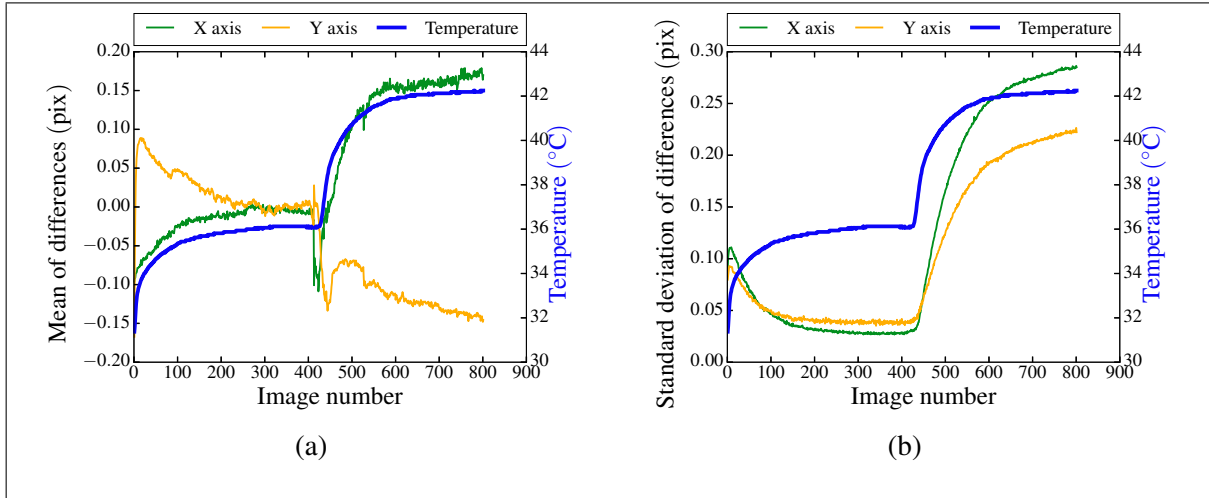


Figure 3.3. Drifts of target positions and temperature variations in each image. The mean and the standard deviation of the differences to the reference catalogue are shown for each image. Image number 360, correspondent to a constant temperature, was set as a reference..

of the differences in the warm-up period reaches 0.11 ± 0.005 pix and 0.09 ± 0.005 pix in X and Y axes, respectively; and with the external heating these values are 0.29 ± 0.005 pix and 0.23 ± 0.005 pix, in X and Y axes.

This effect is due to changes in the geometry of the camera optics; in this case, the thermal expansion coefficient was estimated to be within the range of $93 \cdot 10^{-6}$ m/(mK) to $255 \cdot 10^{-6}$ m/(mK) during the camera warm-up period. This value was calculated considering square pixels with $1.25 \mu\text{m}$ of side length and an expansion in the image plane. This estimation does not match the linear expansion coefficients of the typical camera materials, such as Silicon with $3 \cdot 10^{-6}$ m/(mK), Aluminium with $22.2 \cdot 10^{-6}$ m/(mK), or Glass with $30 \cdot 10^{-6}$ m/(mK). Thus, we conclude that the drift effect is not only produced by thermal expansion of the sensor support, but also by the misalignment of the optical elements of the camera.

Due to the impossibility of using an external temperature controller for some applications, the state of the art in this field has proposed methods to correct the effects of temperature variations after determining the target positions in the images. The drift effect is included in the

calibration model, but it becomes difficult to isolate the effects of temperature on the camera parameters from other unknown systematic effects (Yu et al., 2014). Besides, the model uses discrete values of temperature to calculate camera parameters, thus, some images taken during the camera warm-up period would not have a precise drift compensation. Other authors have proposed a position correction through a drift model (Handel, 2007) which achieves a warm-up correction when the temperature only distorts the image plane while the projection centre remains constant. Thus, the algorithm is only applicable when the camera position is precisely known.

3.2. Temperature stabilization

Adjusting the temperature to a constant level before taking the images helps to avoid further data processing to correct positions drifts. We experimented controlling the temperature using the pixel clock of the camera, which defines the reading speed of the sensor cells. A higher pixel clock value implies a rapid reading of the sensor, and thus a faster transmission of the data to the PC. As a consequence, the temperature of the sensor increases rapidly (Gentele

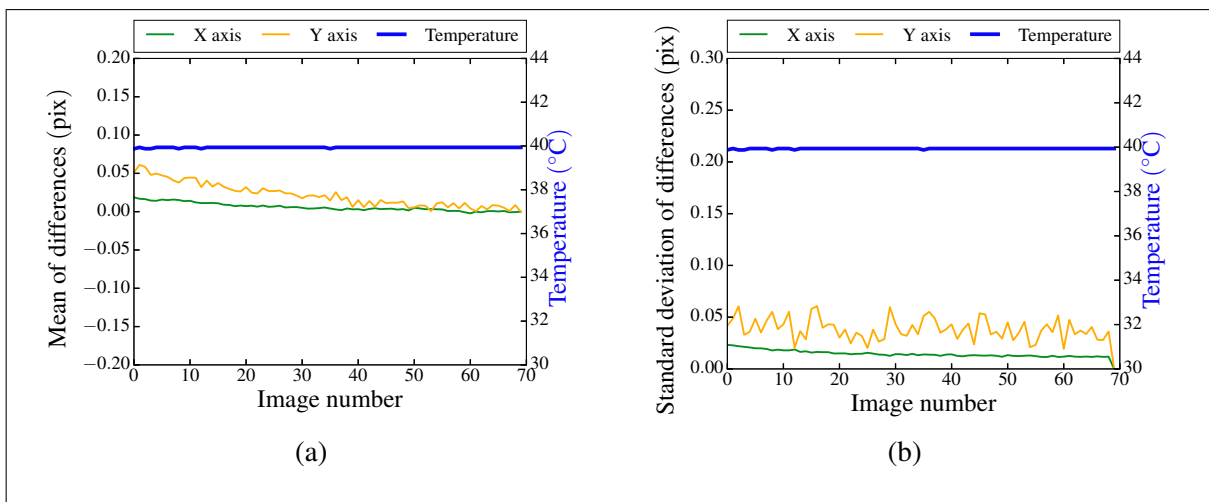


Figure 3.4. Drifts of targets positions in each image after the camera is heated by pixel clock. The mean and the standard deviation of the differences to the reference catalogue are shown for each image at a constant temperature.

& Lewinsky, 2015). Once the temperature reaches the constant value, the pixel clock is set to its initial value, and then the following images are taken at a constant temperature.

As seen in Figure 3.4, this method stabilizes the temperature before the image acquisition. Hence, the calibration images are taken at a constant temperature which reduces the drift of the target positions in the image. The drift shown by the mean of the differences of each target position to the reference is at most 0.02 ± 0.01 pix in X axis and 0.06 ± 0.01 pix in Y axis; and the standard deviation is 0.02 ± 0.004 pix and 0.06 ± 0.01 pix for X and Y axes, respectively. These values are smaller compared to obtained when temperature changed since there is a minimum drift and the targets positions present less dispersion at a constant temperature, as seen in Figure 3.5.

The drift is reduced around 5 times, when the temperature is raised to a constant value using the pixel clock. However, there is still an open question regarding the performance of this method upon very different environmental temperatures, as we expect them to affect

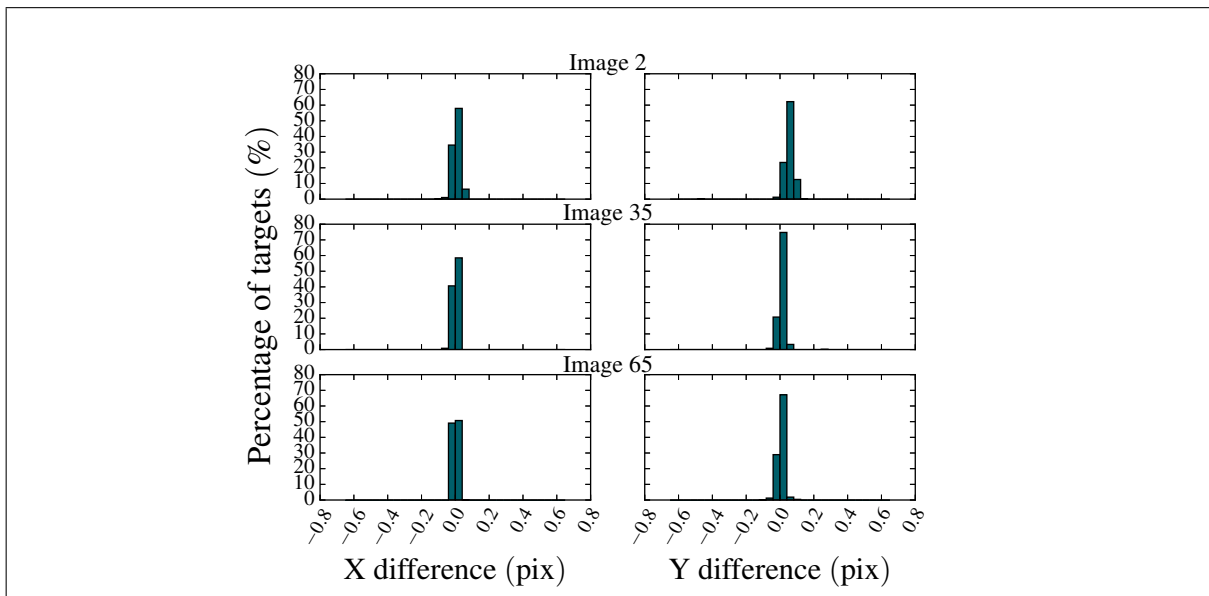


Figure 3.5. Histograms of the differences to the reference in 3 images at a constant temperature. This temperature was achieved after applying the pixel clock method.

the temperature gradient across the camera optics. Thus, calibration should be performed at different temperatures in the range of the operation possibilities. We will leave the study for future works.

This method is also suitable to reduce the time needed for the warm-up, which takes between 20 and 60 minutes. The camera warm-up using a high value of pixel clock takes 7 minutes to reach a constant temperature. Hence, the method is very quick if it is compared to the intrinsic warm-up period of the camera. Thus, the pixel clock solution is suitable to applications that require relatively short response time.

4. TARGETS CHARACTERISTICS OPTIMIZATION

4.1. Dependency on the target type

The calibration targets allow to relate the 3D scene to the 2D pictures through the correspondences between their positions in the ICS and in the WCS. Commonly, the targets are patterns, such as lines, corners and circles; however, the detection accuracy of both lines and corners is affected by the size and orientation of the lines. This makes the calibration dependent on the angle of observation, therefore, circular targets become the most common patterns used in photogrammetry (Heikkilä, 2000). Hence, in this experiment circular white targets are evaluated.

One of the key issues to achieve high accuracy in photogrammetry is the proper extraction of the targets in the images (Luhmann, 2011). The simplest algorithm is to use centroid according to pixel intensities, but later studies have proposed to use contours extractions. Among them, we can find the ellipse centre (Ouellet & Hebert, 2007) or the extractions of another type of target shape, as for example a target whose shape is recognized by Hough transform of circles and lines (Adamos & Faig, 1992). In this thesis, the targets positions are measured with SExtractor, which uses their intensity and shape to estimate their weighted centroid.

In contrast to the detection algorithms, few researchers have paid attention to the physical properties of the targets. Douchamps and Chihara (Douchamps & Chihara, 2009) proposed that large targets are affected by non-linear distortions, but they are better than small targets in terms of noise and discretization. Thus, they developed a new calibration technique that compensates the non-linear distortions and allows to enlarge the target size.

Light reflection is also another characteristic of target construction, as they can be self-illuminated, opaque or retroreflective targets (Shortis & Seager, 2014). These last ones are commonly made of glass spheres that reflect the light back to its original direction and they are the most used type in industrial photogrammetry (Feng et al., 2009). However, the light

received from the targets will be different at different camera locations. Thus, this angle characteristic makes the measured positions of the targets dependent on the observation angle.

We performed an experiment to compare the illumination angle dependency of retroreflective and opaque targets, as well as target size. The objective of this test is proving that the retroreflective condition makes the targets positions in the ICS dependent on the illumination angle, and that opaque and bigger targets are beneficial to reduce this effect. During the stability test, the illumination source is moved to the opposite side of the sensor several times in the Y_w axis of Figure 2.1. A comparison of the illumination angle dependency is made in terms of the images positions for retroreflective and opaque targets of 3 mm and 6 mm.

4.2. Convenient targets characteristics

The dependency on the illumination angle is presented in Figure 4.1, where the measured mean position of the retroreflective targets moves 0.03 ± 0.01 pix and 0.33 ± 0.01 pix in X and Y axes respectively. The differences have a larger dispersion when the images are taken at different illumination angles, this value reaches up to 0.07 ± 0.002 pix in the X axis and 0.11 ± 0.002 pix in the Y direction. This effect is 10 times higher in the direction of Y axis than in X direction since the LEDs array was moved along the Y axis of the camera's image plane. This proves that the targets positions change is a systematic effect produced by the illumination angle variations. Thus, the light received from the retroreflective targets varies with the illumination and the camera's observing angle. As a consequence, the measured targets positions depend on the observation angle.

This angle effect is reduced in the camera calibration process, since the images are taken from several angles around the calibration object. However, the calculation of the extrinsic parameters, depends on the camera location in the WCS. Hence, at the moment they are calculated, it is important to have the scene components fixed. In this case, the illumination angle is decisive in the positions of the targets, which makes inconvenient the use of retroreflective targets. Besides, if the measurements of a photogrammetry system are performed by one

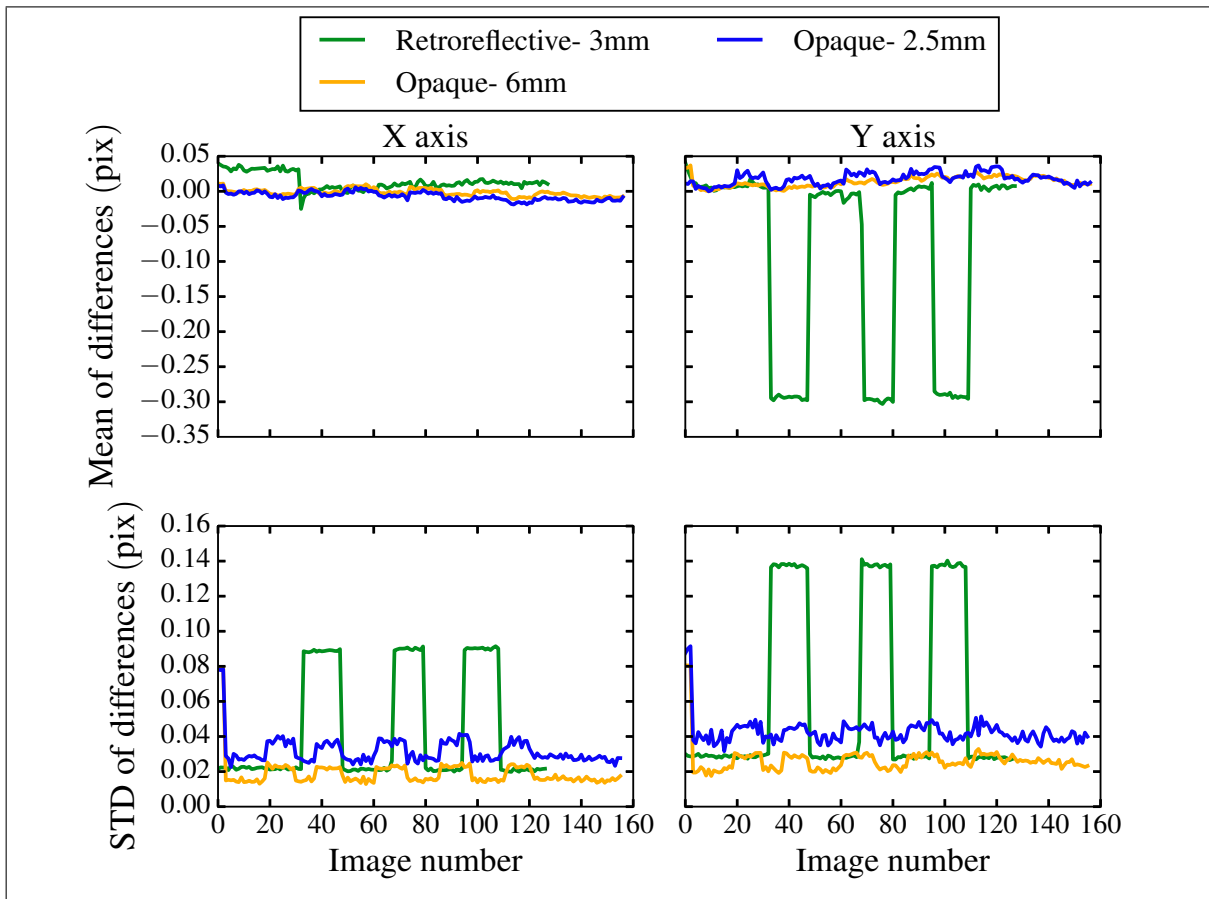


Figure 4.1. Comparison of positions movements dependent on target characteristics, when illumination angle changes 180° . The mean and the standard deviation of the differences to the reference catalogue are shown for each image at independent illumination changes. The retroreflective targets show a higher illumination angle dependency.

fixed camera, the illumination angle will also be important since the deprojection to the WCS is based on the targets ICS positions.

The use of opaque targets reduces the angular dependency by a factor of 10, compared to the retroreflective ones, as seen in Figure 4.1. Even though the measured target displacement along the Y axis for opaque targets is slightly higher than in X axis, the angle effect is reduced to 0.02 ± 0.01 pix and 0.03 ± 0.01 pix in X and Y axes for the 6 mm targets; and to 0.03 ± 0.01 pix and 0.04 ± 0.01 pix for the 3 mm targets. For that reason, the use of opaque

targets instead of retroreflective ones is recommended. They help to reduce the angle dependency in the calculation of the extrinsic parameters and in the photometric measurements of one fixed point of view. Hence, the use of opaque targets relieves the need of using a great quantity of images from different points of view in the camera calibration to compensate for the angle effects.

The use of opaque targets of bigger sizes reduces the illumination angle effect as well. Targets of 6 mm reduce the position changes in 0.01 pix compared to 3 mm targets. As it improves the conditions for the following photometry, it is desirable to enlarge the mentioned area by the use of 6 mm targets instead of 3 mm or smaller targets. Hence, the use of larger targets, or having the camera closer to the calibration plate would lead to have a larger area in the sensor covered by the image of the metrology targets.

5. ILLUMINATION OPTIMIZATION

5.1. Illumination and image quality

Proper illumination conditions improve the whole photogrammetry system since the illumination affects the image quality and the target photometry (Klančar, Kristan, & Karba, 2004; Luhmann, 2011; Lyu, Gao, & Yang, 2017; Wu, Li, Zhang, & Ye, 2016). The exact extraction of the calibration targets in the images becomes difficult with bad lighting conditions (Kang et al., 2008) since low intensities produce a low signal to noise, and high intensities can saturate the images. Thus, a uniform illumination of the cameras' FOV is needed.

The literature proposes many methods to perform a compensation of the illumination effects after the image acquisition process. They are included in the photometry under the name of “invariant to light” methods. Some of them are, modelling the illumination as a Gaussian distribution around the Otsu threshold (Khan, Nisar, Ng, & Lo, 2015) or using a multiplicative reference image to counteract the effect (Klančar et al., 2004). There is also another way to solve the problem, which is managing the illumination in the setup step (Lyu et al., 2017). Muruganantham et al. (Muruganantham et al., 2009) proposed the existence of an optimal value of illumination so that the camera characterization had a better repeatability and precision. In slightly different applications, such as in automated optical inspection systems (AOI), illumination compensation in the setup is achieved using structured illumination. Some of them are, a shape optimization of the physical light (Wu et al., 2016) or a control loop through a projector whose intensity depends on the camera measurements (Lyu et al., 2017).

In this work, we aim at characterizing the variation of the targets positions produced by different illumination intensities in order to reduce them in the image acquisition process. Our proposed photogrammetry application uses a LEDs array to illuminate the FOV of the camera, since they accomplish one of the best performances in terms of lifetime and adaptability (Wu et al., 2016; Liu et al., 2014). For this purpose, the stability test is performed at different illumination intensities. The light intensity is varied in two discrete values with the use of

different current supply given by the Beckhoff system and it is measured in the pixel counts of the targets images and corroborated with the power-meter.

5.2. Illumination advices

Figure 5.1 shows how the standard deviation of the differences to a reference changes with two light intensities, $3.5 \pm 0.03 \mu\text{W} / \text{cm}^2$ to $5.4 \pm 0.2 \mu\text{W} / \text{cm}^2$ measured with the power-meter at one side of the calibration plate. This change produces a pixel intensity variation in the order of 22 %, being the saturated count the complete percentage. There is not an evident movement of the targets in the images, but they present a difference of their positions dispersion of $0.008 \pm 0.003 \text{ pix}$ when light intensity varies. This is a signal to noise effect, since the dispersion in the positions is higher when the pixel counts of the targets are closer to the background counts. The targets move in a random manner when the light intensity changes, which evidences no systematic change in their positions, as seen in Figure 5.1a.

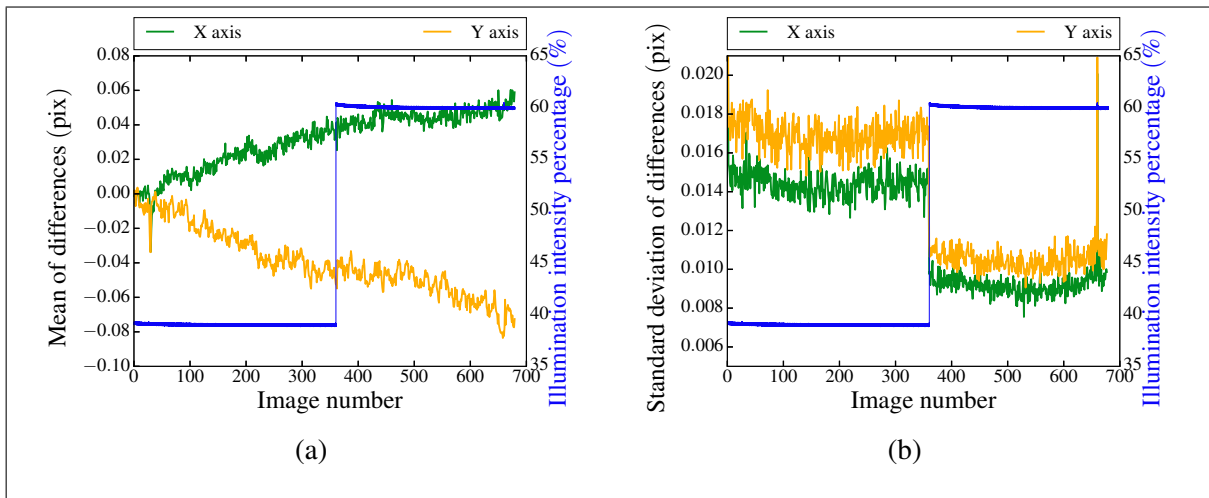


Figure 5.1. Movement of targets positions at two illumination intensities. The blue line presents the illumination in terms of the pixel intensities of the targets images, being the 100 % the value of saturation. The mean of the differences to the reference catalogue number 4 is shown for each image. The standard deviation of the difference to a mean catalogue for each illumination is also presented. No systematic change is seen in the mean value, however, the measurement error is higher when having less signal to noise.

Therefore, the calibration images must be taken under homogeneous illumination conditions to avoid having different dispersion values in the measurement error. Maintaining a uniform illumination in the FOV and in all images, allows all targets to have the same intensity within the linear sensitivity range of the camera. In this range the targets are illuminated so as to ensure high values for the pixel counts in the image but without saturation. There, the Gaussian shape of the targets images helps the following photometry process to be more accurate.

6. CONCLUSIONS

In this work we have demonstrated that the variation of some room conditions change the positions of the targets in the Image Coordinate System. We have found that temperature variations, illumination and target characteristics affect the sub-pixel precision of the target positioning, which is an important step of the camera calibration. Three conditions were evaluated, being the targets reflectivity the one which affected the most the targets positioning in the images. Temperature warm-up produced 0.2 pix of less drift, followed by the illumination intensity whose change implied 25 times less effect than the generated from the temperature. These effects on the targets positioning was estimated to be about 0.5 pix, which implies an error in the focal plane of MOONS in the range of 40 μm to 60 μm . However, the compensations and recommendations proposed in this work reduced the positioning changes to less than 0.1 pix, which corresponds to a range of 8 μm to 12 μm of error in the WCS. The reduction of the positioning movements is within the requirements for MOONS metrology system, hence the goals of this work were achieved. The following subsections show in detail the conclusions of the measured effects and the compensations implemented for each one of the studied conditions.

Temperature

- During the camera warm-up period, a drift of 0.1 pix in the measured positions of the targets was observed. A method based on controlling the camera's pixel clock helped to quickly achieve a constant temperature, which reduces the measured drift to 0.02 pix.
- The pixel clock method also reduces the camera warm-up to just 7 minutes, which is a shorter period of time than the intrinsic camera warm-up of more than 20 minutes.
- The proposed method do not require any external controller to the photogrammetry system. This is beneficial for applications in which the space or the resources are limited, such as MOONS.
- The drift correction is performed in the image acquisition process, before determining the position and characteristics of the targets in the images. This is a novelty in contrast to other methods which model the effect in the calibration algorithms.

- It was also concluded that the original drift is not only produced by thermal expansion of the camera supports in the warm-up period, but camera optical properties are altered with changes of temperature as well.
- Since calibration is affected by temperature changes, it has to be performed at the operation temperature of the entire photogrammetry system. If the photogrammetry system is exposed to a wide range of temperatures, the calibration of the camera at different temperatures is required for high precision results.

Targets Characteristics

- The use of retroreflective targets makes their positioning in the Image Coordinate System highly illumination angle dependent. A difference of position on the order of 0.3 pix is seen when the retroreflective targets are illuminated from opposite locations.
- The use of opaque targets of bigger sizes is recommended in this work. Using opaque targets, the measured drift becomes 10 times smaller compared to the retroreflective ones, and 0.01 pix lesser when the targets are of 6 mm instead of 3 mm diameter.
- A lower dependency to the observation angle is beneficial for reducing the need of taking calibration images from multiple points of view. It is also useful for avoiding the illumination angle dependency in the estimation of the extrinsic parameters and in the performance of photogrammetric measurements with a camera that remains in the same position in the WCS.
- The angle effect is also controllable if the source of illumination is fixed to the metrology camera. However, this practice could produce an non-homogeneous illumination in the field of view of the camera.

Illumination Intensity

- A 22 % of different light intensity makes the dispersion of the targets positions change around 0.008 pix due to differences in the signal to noise ratio. For that reason, it is advisable for achieving micrometric accuracy, to have an homogeneous illumination in the field of view of the camera and in all calibration images.

REFERENCES

- Adamos, C., & Faig, W. (1992). Hough transform in digital photogrammetry. In *Xviiith isprs congress technical commission iii: Mathematical analysis of data* (Vol. XXIX, p. 250). Retrieved from http://www.isprs.org/proceedings/XXIX/congress/part3/250_XXIX-part3.pdf
- Bacakoglu, H., & Kamel, M. S. (1997). A three-step camera calibration method. *IEEE Transactions on Instrumentation and Measurement*, 46(5), 1165-1172. (ID: 1) doi: 10.1109/19.676732
- Bazargani, H., & Laganiere, R. (2015, December). Camera calibration and pose estimation from planes. *IEEE Instrumentation Measurement Magazine*, 18(6), 20-27. doi: 10.1109/MIM.2015.7335834
- Bertin, E. (2014). *Source extractor*. Retrieved from <http://www.astromatic.net/software/sextactor>
- Bouguet, J.-Y. (2015). *Camera calibration toolbox for matlab*. Retrieved from https://www.vision.caltech.edu/bouguetj/calib_doc/index.html#ref
- Brown, D. C. (1971). Close-range camera calibration. *PHOTOGRAMMETRIC ENGINEERING*, 37(8), 855–866.
- Cirasuolo, M., Afonso, J., Carollo, M., Flores, H., Maiolino, R., Oliva, E., ... Zoccali, M. (2014). *Moons: the multi-object optical and near-infrared spectrograph for the vlt* (Vol. 9147). Retrieved from <http://dx.doi.org/10.1117/12.2056012> doi: 10.1117/12.2056012

- Douxchamps, D., & Chihara, K. (2009). High-accuracy and robust localization of large control markers for geometric camera calibration. *IEEE Transactions on Pattern Analysis and Machine Intelligence*, 31(2), 376-383. (ID: 1) doi: 10.1109/TPAMI.2008.214
- Drass, H., Vanzi, L., Torres-Torriti, M., Dünner, R., Shen, T.-C., Belmar, F., ... Fairley, A. (2016). Implementation of the metrology system for moons. In *Ground-based and airborne instrumentation for astronomy vi* (Vol. 9908). doi: 10.1117/12.2232654
- Feng, Q., Li, Z., Chen, X., & Li, G. (2009, Oct). Fast recognition and precise centering of artificial targets. In *2009 2nd international congress on image and signal processing* (p. 1-4). doi: 10.1109/CISP.2009.5304651
- Gentele, M., & Lewinsky, A. (2015). *Ids cameras: Techtip: Bandwidth management with adjustable pixel clock*. Germany: IDS Imaging Development Systems GmbH. Retrieved from <https://en.ids-imaging.com/manuals-ueye.html>
- Handel, H. (2007). Analyzing the influences of camera warm-up effects on image acquisition. In Y. Yagi, S. B. Kang, I. S. Kweon, & H. Zha (Eds.), (Vol. 4844, p. 258). Tokyo, Japan: - Springer Berlin Heidelberg. (ID: - Handel2007) doi: 10.1007/978-3-540-76390-1_26
- Haynes, R., Barden, S., de Jong, R., Schnurr, O., Bellido, O., Walcher, J., ... Ansgorge, W. (2014). *The 4most instrument concept overview* (Vol. 9147). Retrieved from <http://dx.doi.org/10.1117/12.2057253> doi: 10.1117/12.2057253
- Healey, G. E., & Kondepudy, R. (1994, Mar). Radiometric ccd camera calibration and noise estimation. *IEEE Transactions on Pattern Analysis and Machine Intelligence*, 16(3), 267-276. doi: 10.1109/34.276126
- Heikkilä, J. (2000, Oct). Geometric camera calibration using circular control points. *IEEE Transactions on Pattern Analysis and Machine Intelligence*, 22(10), 1066-1077.

doi: 10.1109/34.879788

Heikkilä, J., & Silvés, O. (1997). A four-step camera calibration procedure with implicit image correction. In *Proceedings of the 1997 IEEE Computer Society Conference on Computer Vision and Pattern Recognition* (p. 1106). doi: 10.1109/CVPR.1997.609468

Iraf. (n.d.). *Daofind*. Retrieved from <http://iraf.net/>

Kang, D. J., Ha, J. E., & Jeong, M. H. (2008). Detection of calibration patterns for camera calibration with irregular lighting and complicated backgrounds. *International Journal of Control, Automation and Systems*, 6(5), 746-754.

Khan, M. B., Nisar, H., Ng, C. A., & Lo, P. K. (2015, Nov). Illumination compensated segmentation of microscopic images of activated sludge flocs. In *2015 International Conference on Digital Image Computing: Techniques and Applications (DICTA)* (p. 1-5). doi: 10.1109/DICTA.2015.7371265

Klančar, G., Kristan, M., & Karba, R. (2004, 2/29). Wide-angle camera distortions and non-uniform illumination in mobile robot tracking. *Robotics and Autonomous Systems*, 46(2), 125-133. doi: <https://doi-org.ezproxy.puc.cl/10.1016/j.robot.2003.11.001>

Liu, J., z. Zhang, B., Liu, H., s. Zeng, S., q. Zhao, W., & g. Lu, L. (2014). Impact of detector spatial uniformity on the measurement of averaged led intensity. *IEEE Photonics Journal*, 6(1), 1-7. (ID: 1) doi: 10.1109/JPHOT.2013.2295458

Luhmann, T. (2011). *3d imaging: how to achieve highest accuracy* (Vol. 8085). doi: 10.1117/12.892070 [doi]

Lyu, C., Gao, S., & Yang, J. (2017, 6). An optimisation design of adaptive illumination for a multi-reflective 3d scene. *Optics and Lasers in Engineering*, 93, 128-138. doi: <https://doi-org.ezproxy.puc.cl/10.1016/j.optlaseng.2017.02.001>

Montgomery, D., Atkinson, D., Beard, S., Cochrane, W., Drass, H., Guinouard, I., ... Watson, S. (2016). *Development of the fibre positioning unit of moons* (Vol. 9908). Retrieved from <http://dx.doi.org/10.1117/12.2234183> doi: 10.1117/12.2234183

Muruganantham, C., Jawahar, N., Ramamoorthy, B., & Giridhar, D. (2009, 09/15). Optimal settings for vision camera calibration. *International Journal of Advanced Manufacturing Technology*, 42(7), 736-748. Retrieved from <http://search.ebscohost.com/login.aspx?direct=true&db=a9h&AN=39563869&lang=es&site=ehost-live> doi: 10.1007/s00170-008-1634-y

OpenCV. (2016). *Camera calibration and 3d reconstruction*. Retrieved from http://docs.opencv.org/2.4/modules/calib3d/doc/camera_calibration_and_3d_reconstruction.html

Ortiz, A., & Oliver, G. (2004). Radiometric calibration of ccd sensors: dark current and fixed pattern noise estimation. In *Robotics and automation, 2004. proceedings. icra '04. 2004 ieee international conference on* (Vol. 5, p. 4730-4735 Vol.5). (ID: 1) doi: 10.1109/ROBOT.2004.1302465

Ouellet, J. N., & Hebert, P. (2007, May). A simple operator for very precise estimation of ellipses. In *Computer and robot vision, 2007. crv '07. fourth canadian conference on* (p. 21-28). doi: 10.1109/CRV.2007.8

Pasquini, L., Avila, G., Blecha, A., Cacciari, C., Cayatte, V., Colless, M., ... Zoccali, M. (2002, December). Installation and commissioning of FLAMES, the VLT Multifibre Facility. *The Messenger*, 110, 1-9.

Podbreznik, P., & Potočnik, B. (2008). Influence of temperature variations on calibrated

cameras. *International Journal of Electrical, Computer, Energetic, Electronic and Communication Engineering*, 2(5), 719 - 725. Retrieved from <http://waset.org/Publications?p=17>

Samper, D., Santolaria, J., Brosted, F. J., Majarena, A. C., & Aguilar, J. J. (2013). Analysis of tsai calibration method using two- and three-dimensional calibration objects. *Machine Vision and Applications*, 24(1), 117–131. Retrieved from <http://dx.doi.org/10.1007/s00138-011-0398-9> doi: 10.1007/s00138-011-0398-9

Schenk, T. (2005). Introduction to photogrammetry.

Semeniuta, O. (2016). Analysis of camera calibration with respect to measurement accuracy. *Procedia CIRP*, 41, 765 - 770. Retrieved from <http://www.sciencedirect.com/science/article/pii/S2212827115011877> doi: <http://dx.doi.org/10.1016/j.procir.2015.12.108>

Sentenac, T., Maoultt, Y. L., Rolland, G., & Devy, M. (2003, Feb). Temperature correction of radiometric and geometric models for an uncooled ccd camera in the near infrared. *IEEE Transactions on Instrumentation and Measurement*, 52(1), 46-60. doi: 10.1109/TIM.2003.809103

Shortis, M. R., & Seager, J. W. (2014, Sep). A practical target recognition system for close range photogrammetry. *Photogrammetric record*, 29(147), 337-355. (Article)

Smith, M., & Cope, E. (2012). *The effects of temperature variation on single-lens-reflex digital camera calibration parameters* (Tech. Rep.). Retrieved from <http://www.isprs.org/proceedings/XXXVIII/part5/papers/158.pdf>

Swapna, P., Krouglicof, N., & Gosine, R. (2009, May). The question of accuracy with geometric camera calibration. In *2009 canadian conference on electrical and computer*

engineering (p. 541-546). doi: 10.1109/CCECE.2009.5090189

Tamura, N., Takato, N., Shimono, A., Moritani, Y., Yabe, K., Ishizuka, Y., ... Yasuda, N. (2016). *Prime focus spectrograph (pfs) for the subaru telescope: overview, recent progress, and future perspectives* (Vol. 9908). Retrieved from <http://dx.doi.org/10.1117/12.2232103> doi: 10.1117/12.2232103

Torres-Torriti, M., Vanzi, L., Dünner, R., Belmar, F., Dauvin, L., Shen, T.-C., ... Cabral, A. (2014). The metrology system for the multi-object optical and near-infrared spectrograph moons. In *Ground-based and airborne instrumentation for astronomy v* (Vol. 9147). (10.1117/12.2055686) doi: 10.1117/12.2055686

V-stars/n. (n.d.). GSI. Retrieved from <https://www.geodetic.com/f.ashx/BROCHURES/V-STARS-N-Brochure.pdf>

Wang, H., Shen, S., & Lu, X. (2012, June). Comparison of the camera calibration between photogrammetry and computer vision. In *2012 international conference on system science and engineering (icsse)* (p. 358-362). doi: 10.1109/ICSSE.2012.6257207

Wang, S.-Y., Chou, R. C. Y., Huang, P.-J., Ling, H.-H., Karr, J., Chang, Y.-C., ... Shimono, A. (2016). *Metrology camera system of prime focus spectrograph for suburu telescope* (Vol. 9908). Retrieved from <http://dx.doi.org/10.1117/12.2232035> doi: 10.1117/12.2232035

Winkler, R., Barden, S. C., & Saviuk, A. (2016). *4most metrology system image processing* (Vol. 9908). Retrieved from <http://dx.doi.org/10.1117/12.2233257> doi: 10.1117/12.2233257

Wu, F., Li, S., Zhang, X., & Ye, W. (2016). A design method for leds arrays structure illumination. *Journal of Display Technology*, 12(10), 1177-1184. (ID: 1) doi: 10.1109/JDT.2016.2593770

Yang, X., Fang, S., Kong, B., & Li, Y. (2014). Design of a color coded target for vision measurements. *Optik - International Journal for Light and Electron Optics*, 125(14), 3727-3732. doi: 10.1016/j.ijleo.2014.03.009

Yu, Q., Chao, Z., Jiang, G., Shang, Y., Fu, S., Liu, X., ... Liu, H. (2014, 12). The effects of temperature variation on videometric measurement and a compensation method. *Image and Vision Computing*, 32(12), 1021-1029. doi: <http://dx.doi.org.ezproxy.puc.cl/10.1016/j.imavis.2014.08.011>

Zhang, Z. (2000). A flexible new technique for camera calibration. *IEEE Transactions on Pattern Analysis and Machine Intelligence*, 22(11), 1330-1334. (ID: 1) doi: 10.1109/34.888718